Appl Phys B (2009) 97: 607–618
DOI 10.1007/s00340-009-3605-x

Applied Physics B
Lasers and Optics

Excitation pathways and efficiency of Eu ions in GaN by site-selective spectroscopy

Z. Fleischman · C. Munasinghe · A.J. Steckl · A. Wakahara · J. Zavada · V. Dierolf

Received: 9 March 2009 / Revised version: 15 May 2009 / Published online: 18 June 2009

Abstract Using combined excitation emission spectroscopy, we performed a comparative study of europium ions in GaN in samples that have been in situ doped during interrupted growth epitaxy (IGE) or conventional molecular beam epitaxy (MBE) as well as samples that were grown using organometallic vapor phase epitaxy (OMVPE) and subsequently ion implanted with Eu ions. Through site-selective resonant excitation, we are able to unambiguously assign all major observed transitions to a combination of different incorporation sites and electron–phonon coupled transitions. We identified at least nine different incorporation sites of Eu ions in GaN and studied how these sites behave under different excitation conditions and how their relative number is modified by different growth and doping conditions. The coupling to phonons has also been studied for a series of $Al_xGa_{1-x}N$ samples with $x = 0 \ldots 1$. We find that a main site most resembling an unperturbed Eu ion on Ga site is always dominant, while the minority sites are changing substantially in relative numbers and can occur in some samples fairly close in emission intensity to the main site. In terms of the excitation pathway after the creation of electron-hole pairs, we found three types of centers: (1) sites that are dominantly excited through shallow defect traps; (2) sites that are excited through a deep defect trap; (3) sites that cannot be excited at all including the majority of the main sites. We interpret this finding to indicate that the ion in this environment is not very efficient in trapping excitation and that the indirect excitation involving other traps depends on the ion/trap distance. Many of the main sites are far away from these traps and cannot be excited through this channel at all. The efficiency of excitation is highest for the deep traps, indicating that it would be desirable to enrich the respective site, as has been done with some success in the IGE grown samples.

PACS 71.55.Eq · 71.70.Ch · 78.55.Cr · 78.60.Hk

1 Introduction

Europium ions in GaN have attracted considerable attention in the semiconductor laser community due to the recent success in realizing both efficient electroluminescence (EL) devices and laser action under optical excitation [1–5]. However, lasing under electrical excitation has not been obtained so far. In the laser experiments, an interesting change of laser wavelength has been observed under variation of the length of the excitation channel, indicating a critical role of different incorporation sites [5]. After growth, the first evaluation of material quality as an EL material is usually done by measuring the photoluminescence (PL) intensity excited with photon energies above the bandgap of GaN. While being a good measure for the merit of the sample under study for EL, such measurements are not site selective and the

Z. Fleischman · V. Dierolf (✉)
Physics Department, Lehigh University, Bethlehem, PA 18015, USA
e-mail: vod2@lehigh.edu

C. Munasinghe · A.J. Steckl
Nanoelectronics Laboratory, University of Cincinnati, Cincinnati, OH 45221-0030, USA

A. Wakahara
Department of Electrical and Electronic Engineering, Toyohashi University of Technology, 1-1 Hibarigaoka, Tempaku, Toyohashi 441-8580, Japan

J. Zavada
U.S. Army Research Office, Durham, NC 27709, USA

spectra show overlapping contributions that are hard to analyze. To make this point, we show in Fig. 1 three different spectra taken from GaN:Eu samples produced with different growth conditions. For the depicted $^5D_0$ to $^7F_2$ transition, a maximum of three peaks is expected for the C_{3v} symmetry of the Ga site in GaN. The observed additional peaks could be caused by various mechanisms such as different sites, excitation from other states, and electron–phonon coupled transitions. Excitation spectra observed by Hömmerich et al. [6] added to the complication. In the spectral region of the $^7F_0$ to $^5D_0$ excitation transition five excitation peaks instead of a single peak were observed. The large shifts amongst peaks make it unlikely that we are dealing only with different sites. Detailed studies by Peng et al. [7] using time-dependent measurements revealed clearly different sites and excitation pathways, but some peak assignments remained tentative. The process is even more complex due to the presence of different excitation pathways involving defect traps, as directly demonstrated in [8]. Recent publications [9, 10] revealed a site dependence of these pathways. In order to conclusively determine the origin of each of these peaks and its site-specific excitation pathway, detailed site-selective PL measurements must be carried out. To this end, we use our technique of combined excitation emission spectroscopy (CEES) and address the following tasks:

- Identify different sites and create a fingerprint of their energy levels.
- Identify electron–phonon coupled transitions and determine coupling strength.
- Determine the influence of the growth conditions on the site distribution.
- Determine the relation between non-resonant and resonant excitation schemes and determine the participation of each site in these schemes.

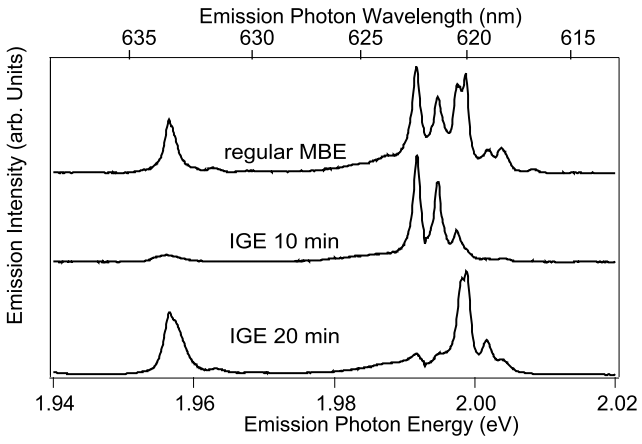

Fig. 1 Emission spectra due to the Eu $^5D_0$ to $^7F_2$ transition obtained under above GaN bandgap 351 nm excitation for samples grown under different conditions. Sample Type 1 with indicated shutter times

- Relate the results to the less detailed earlier site-selective studies [5, 7, 10].

2 Experimental techniques and samples information

The site-selective PL characterization of the Eu-doped GaN samples was carried out utilizing several different excitation-emission schemes, which are indicated in Fig. 2. For the resonant excitation of the Eu levels, we use our technique of CEES. In this technique, already successfully used for Nd^{3+} and Er^{3+} in GaN [11, 12], we record a large number of emission spectra for a sequence of excitation energies. The resulting 2-D data set of emission intensity as a function of excitation and emission photon energy is conveniently depicted using image and/or contour plots. In addition, we explored several non-resonant excitation methods using above bandgap excitation with a 351 nm Argon laser, below bandgap excitation with a 405 nm InGaN laser, and excitation with energetic electrons in an electron microscope.

We have used for our studies a variety of samples with different growth conditions, doping methods, and substrates. We categorize them as follows:

Sample Type 1 These samples, for which the majority of the measurements were performed, were produced in the Nanoelectronics Laboratory at the University of Cincinnati using the interrupted growth epitaxy (IGE) technique as described in [3]. In this method, the film is exposed for 5 min to only the flow of nitrogen while the gallium beam is interrupted. The *total* time that the gallium beam is on is kept

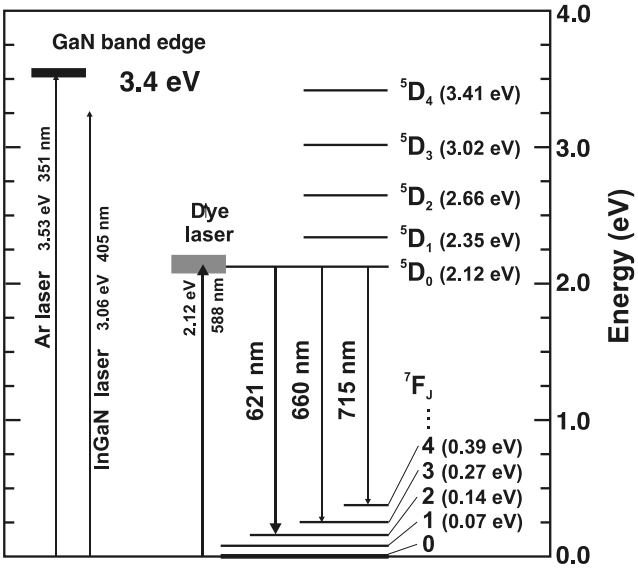

Fig. 2 Schematic of energy levels of Eu ions in GaN and transitions relevant for site-selective spectroscopy studies

constant, but the on/off period is varied while the time it is open in each cycle is varied. The samples are labeled according to the time the Ga beam is open during each cycle. The sample labeled 60 min is essentially a regular MBE sample (and will be labeled as such), while for the one labeled e.g. 10 min, a cycle of 10 min Ga beam open and 5 min closed is repeated 6 times. MBE growth parameters were Ga cell at 900°C with a beam equivalent pressure (BEP) of $\sim 4.1 \times 10^{-7}$ Torr and Eu cell at 440°C. The Eu incorporation in the films was found to be ~0.1 at%, which is below the onset of luminescence concentration quenching [13]. The growth was carried out at 650°C for Si substrates. The RF nitrogen plasma was set at a gas flow of 1.8 sccm with 400 W forward power to achieve the optimum growth condition. The samples were grown on silicon substrates and have also been studied by other groups [7, 9, 10, 14–16], allowing us to link our measurements with other published data.

Sample Type 2 The samples were grown by MBE on *c*-plane sapphire substrates. A low temperature, 50 nm thick AlN buffer was followed by growth of ~0.5 µm of GaN:Eu at 800°C with a Eu cell temperature of 470°C. The Ga flux during growth was varied from 3.0×10^{-7} to 5.4×10^{-7} Torr by controlling the Ga cell temperature in the range of 860–890°C. The samples were capped with an additional 50 nm of low temperature AlN and annealed at 675°C for 100 min. This produces a Eu concentration in the range of 0.12 at%. These samples were also used to determine the ferromagnetic properties of these RE-doped samples [17].

Sample Type 3 This sample type consists of a series of $Al_xGa_{1-x}N$ samples with varying aluminum concentration ($0 < x < 1$) produced at the Toyohashi University of Technology in Japan [16]. $Al_xGa_{1-x}N$ layers of thickness 1–2 µm were grown on c-plane sapphire substrates at 1100°C in 76 Torr by organometallic vapor phase epitaxy (OMVPE). The samples were implanted with 200 keV Eu^{3+} ions at a dose of 10^{15} cm^{-2} at room temperature. The projected range and peak Eu^{3+} concentration were estimated to be approximately 100 nm and 0.3 at%, respectively. After the implantation, the samples were subjected to a rapid thermal anneal (RTA) at 1100°C for 2 minutes in N_2 atmosphere. For details see [18].

Using such a wide variety of samples allows a good characterization of the dependence of the incorporation of Eu^{3+} as a function of growth parameters and will allow us to link our results to already-published data that exhibit a somewhat confusing site multiplicity.

3 Experimental results and discussion

3.1 Energetic fingerprints of different sites

For our CEES studies, we chose the $^7F_0$ to $^5D_0$ transition for excitation due to its simplicity. Since both of these are $J = 0$ levels, no crystal field splitting will exist under any kind of symmetry, and any site that exists for this excitation transition should only demonstrate one excitation peak. Resonant excitation was performed for this transition using a tunable dye laser operating in the region of 2.095–2.183 eV (568–592 nm). For emission, we focused mainly on the $^5D_0$ to $^7F_2$ transition, which has been shown to have the highest emission intensity and which also is very important technologically as the source of red emission in these samples. Measurements were also conducted on the $^5D_0$ to $^7F_3$ transition for comparison. In Fig. 3, the CEES data for our MBE sample (60 min) of Sample Type 1 are presented for the $^5D_0$ to $^7F_2$ transition. Immediately apparent is the richness of the data present in this image, which depicts the wide variety of different emission structures present in this region. There are four emission peaks that show up as vertical bands in the image (two fairly strong ones at 1.956 and 1.997 eV, and two

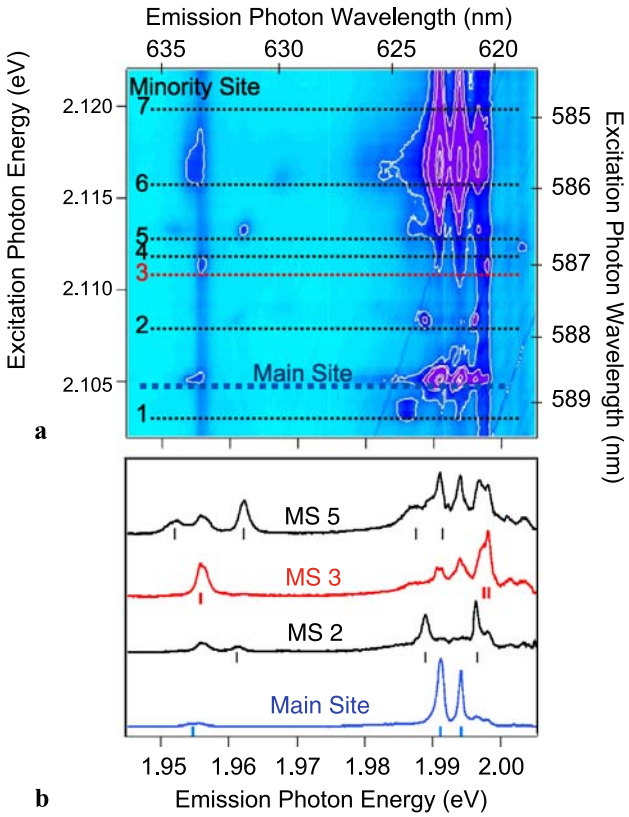

Fig. 3 Image plot CEES data for $^5D_0$ to $^7F_2$ emission and $^5D_0$ to $^7F_0$ excitation obtained for a regular MBE sample grown on glass. (Sample 1, 60 min.) MBE-grown sample that has been in situ doped with Eu ions. Different sites are indicated with *dashed lines*. Selected emission spectra under resonant excitation are shown on the *left*

relatively weaker ones at 2.0018 and 2.0039 eV), indicating that they can be excited over the entire range of energies presented. These will be discussed further in Sect. 3.4, when we deal with these non-resonant excitation channels. In addition, there are a variety of different emission peaks that occur at discrete excitation energies. The changes in emission peak structure with excitation energy in this image clearly show the multi-site structure of the Eu ions in this sample. Assigning the peaks to different sites and/or transitions is a challenging task made more difficult by the sheer number of origins of the different emissions. We make use of the fact that a particular site will yield its own unique emission spectra in terms of both line position and relative intensity. In this way, we are able to identify a total of eight different Eu incorporation sites whose excitation energies are indicated by the dotted lines. We identify the main site and label the remaining sites 1 to 7 in order of ascending excitation energy. For further reference, we highlight the main site in blue and the minority site MS 3 in red.

Figure 3(b) shows several of these unique emission spectra for a few of the different Eu sites. The two most dominant excitation peaks shown in the CEES image occur at 2.105 eV and 2.117 eV. For both we obtain identical emission spectra. We identify the lower energy as the main site and the higher we assign to electron–phonon coupling, which we will discuss in more detail in Sect. 3.2. The other seven Eu sites fall under the classification of minority sites, whose emission intensities are typically much lower than that of the majority site. The identified peak positions for all eight sites are given in Table 1, which also includes the peak positions obtained from CEES measurements of the $^5D_0$ to $^7F_3$ transition.

The main site produces the most intense emission peaks in the region studied, and hence it is reasonable to assume that we are dealing with Eu ions that occupy a substitutional Ga lattice site, placing the dopant into C_{3v} symmetry. In this case we expect three emission lines for the $^5D_0$ to $^7F_2$ transition, two lines at a higher transition energy corresponding to the two lower crystal field levels and one line at a lower transition energy corresponding to the one higher crystal field level. This expectation matches very well with the emission spectra. It should be noted that the peak at 1.9550 eV (634.27 nm) has been glanced over or assigned to the $^5D_1$ to $^7F_4$ transition [7, 19, 20]. We can exclude the latter assignment in our measurements since the peak appears already under excitation of the $^5D_0$ state at low excitation intensities such that the $^5D_1$ level will not be excited at all.

As shown in Table 1, the minority sites produce anywhere from one to four emission peaks for the $^5D_0$ to $^7F_2$ transition. (It should be noted that these are "identified" emission peaks and that there could be more peaks associated with a particular site that are hidden under the peaks of other sites.) The unique spectral signatures of the different incorporation sites indicate a unique local environment for the emitting europium ion. These environments could involve europium ions in the proximity of ion vacancies, interstitials, or other intrinsic defects in the host lattice. It is also extremely likely that some of these different sites could represent europium on the Ga substitutional lattice location that is being perturbed by a nearby defect. Also worth mentioning is that the main site and minority site 1,2 correspond quite well to the three lowest energy excitation peaks identified by Hömmerich's group in their studies of this transition region [6]. The integrated PL intensity for each site is shown in Fig. 4.

Table 1 Peak positions determined for nine sites for Eu in GaN, Sample Type 1. All values are given in eV. Transitions labeled with * are associated with an electron–phonon coupled transitions. The corresponding labels of the most apparent sites used in other publications are included as well

Transition	Main Site	MS 1	MS 2	MS 3	MS 4	MS 5	MS 6	MS 7	MS 8
Refs.:									
[5]	Eu_x			Eu_y					
[7]	Site 1			Site 2			Site 3		
[10]	Eu_1			Eu_{2m}					Eu_{2I}
$^7F_0$ to $^5D_0$	2.171*	2.1042	2.1091	2.1124	2.1131	2.1142	2.1171*	2.1211	
	2.117*						2.1091		
	2.1059								
$^5D_0$ to $^7F_3$	1.8735	1.8574	1.8715	1.8700	1.8719	1.8832	1.8845	1.8939	
	1.8678		1.8687	1.8691	1.8645	1.8816			
	1.8641		1.8648			1.8672			
			1.8624			1.8557			
$^5D_0$ to $^7F_2$	1.9947	1.9868	1.9968	1.9986	2.0036	1.9966	1.9684	2.0092	1.9969
	1.9917		1.9894	1.9976	2.0014	1.9899		1.9880	1.9940
	1.9550		1.9679	1.956	1.9599	1.9627		1.9716	
						1.9528			

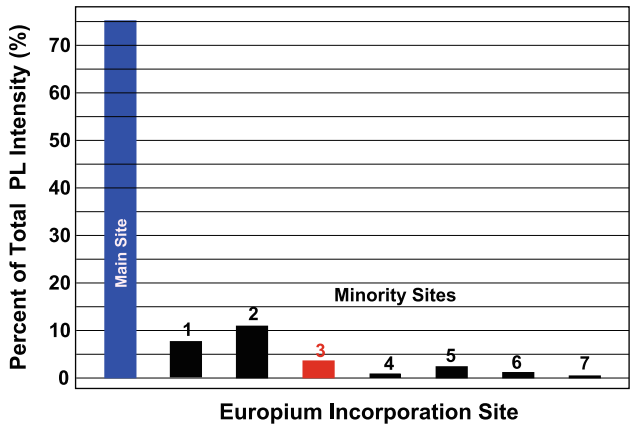

Fig. 4 Photoluminescence intensity of the various identified Eu incorporation sites integrated over the region of the $^5D_0$ to $^7F_2$ transition. Measurements were performed on regular MBE sample grown on glass. (Sample 1, 60 min.)

The main site contributes about 75% of the total emission while several minority sites produce emissions on the order of one-tenth that of the main site. Most of the minority sites produce even lower intensities. It should be noted that these intensities only roughly indicate the relative abundance of the different europium sites due to the lack of information about the differences in transition probabilities and branching ratios. Due to the forbidden character of the $^7F_0$ to $^5D_0$ transition, we suspect that the least perturbed main site has the lowest transition probability and its abundance may hence be underestimated. The ratio between main site and minority sites may well be similar to the one observed for Nd-doped samples that have been grown under similar conditions [11].

Comparing our sites with the ones that participate in optical gain under UV excitation [5], we find that predominantly the main site and the MS 3 are contributing and suspect that the site labeled Eu_x corresponds to the main site while Eu_y corresponds to MS 3.

3.2 Electron–phonon coupling

In assigning the excitation peaks we have left out the higher energy peaks that are not expected for the single transition that we considered. We will deal with them in the following and show that they are related to electron–phonon coupling. In the spectral range of the $^7F_0$ to $^5D_0$ transition (590–570 nm), we find three distinct excitation peaks, which, as we show in Fig. 5, exhibit exactly the same emission spectrum that is characteristic for the main site. For this reason, we can exclude a different site as the origin. The excitation peaks are quite different in spectral width (0.7, 3.1, 0.4 meV for the peaks at 2.105, 2.117, and 2.171 eV, respectively).

We need to consider electron–phonon coupling here, which, due to the forbidden character of the transition, could

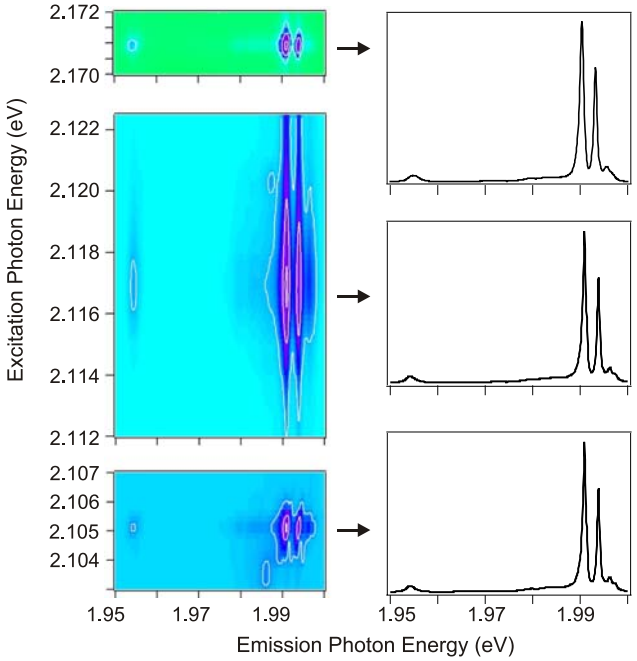

Fig. 5 (*Left*) CEES image/contour plots of the $^5D_0$ to $^7F_2$ transition region for three different excitation energies associated with the $^5D_0$ to $^7F_0$ transition. (*Right*) emission spectra associated with each of these excitation peaks. Measurements were performed on regular MBE sample grown on glass. (Sample 1, 60 min.)

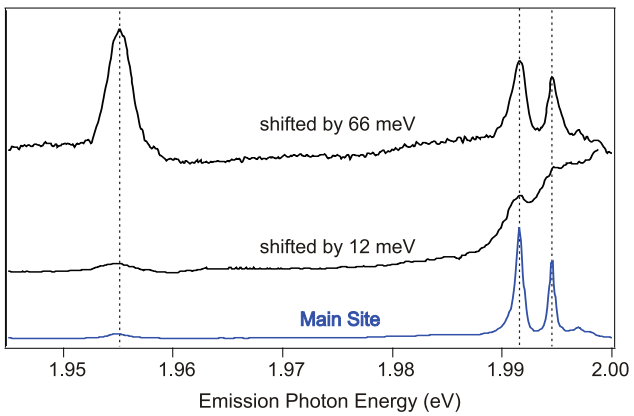

Fig. 6 Two phonon replicas of the red emission from the main site 2. The replicas are shifted by 12 meV and 66 meV from the zero-phonon emission. Measurements were performed on regular MBE sample grown on glass. (Sample 1, 60 min.)

lead to relatively more pronounced features. The dynamic mixing induced by the vibrational mode leads to admixing of states for which transitions are allowed. In order to confirm the corresponding energy shifts, we need to look for the phonon replica in the emission spectrum as well. By closer inspection of the data presented in Fig. 3, we can find such features shifted by 66 meV and 12 meV, just as in the excitation spectrum. We show the corresponding shifted spectra in Fig. 6. The shift of 66 meV corresponds closely to the GaN

LO phonon energy. The replica that is shifted by 12 meV has not been reported before and most likely originates from a phonon mode that is localized to the Eu majority incorporation site. This would account for the homogeneous broadening of the excitation peak associated with this phonon mode. We have found a mode of similar energy for Nd as well [11]. The emission transition meets the requirement to determine the coupling strength in the weak coupling approximation by determining the ratio of zero-phonon line to the first phonon sideband. The coupling determined that way is rather weak for both modes, having a Huang-Rhys factor S of approx 0.01.

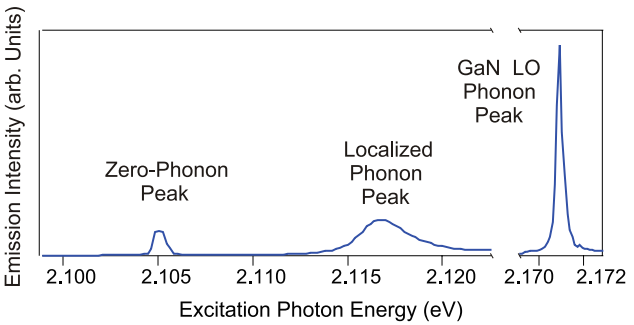

Fig. 7 Integrated excitation spectrum of the $^5D_0$ to $^7F_2$ emission transition showing the zero-phonon excitation line at 2.105 eV as well as the localized-phonon-assisted excitation peak at 2.112 eV and the GaN LO phonon-assisted peak at 2.171 eV. Measurements were performed on regular MBE sample grown on glass. (Sample 1, 60 min.)

Despite such weak electron–phonon coupling in these samples, the data show a very efficient phonon-assisted excitation mechanism involving both types of observed phonon transitions, as seen in the excitation spectrum shown in Fig. 7. We find that the total emission intensity of the localized-phonon-assisted excitation is 7× larger than that of the zero-phonon excitation, while the total emission intensity of the GaN LO phonon-assisted excitation is 3× larger than that of the zero-phonon excitation.

To further confirm our assignment and to study the coupling phenomena in more detail, we investigated the evolution of these excitation peaks as a function of aluminum concentration. A series of $Al_xGa_{1-x}N$-alloy samples with varying aluminum concentration ($0 < x < 1$) was produced for that purpose (Sample Type 3). In Fig. 8, we show the CEES images for this series of sample focusing on the main site. The zero-phonon line as well as the sidebands associated with the localized phonon and the GaN LO phonon can be found for all compositions. The phonon-coupled transitions become relatively weaker at first but increase again as we approach AlN. This may be explained by the degree of order in the samples due to the alloying. In the case of GaN and AlN the zero-phonon line is forbidden such that the phonon-coupled transitions dominate. In the disordered alloys, the zero-phonon lines are stronger by themselves already due to

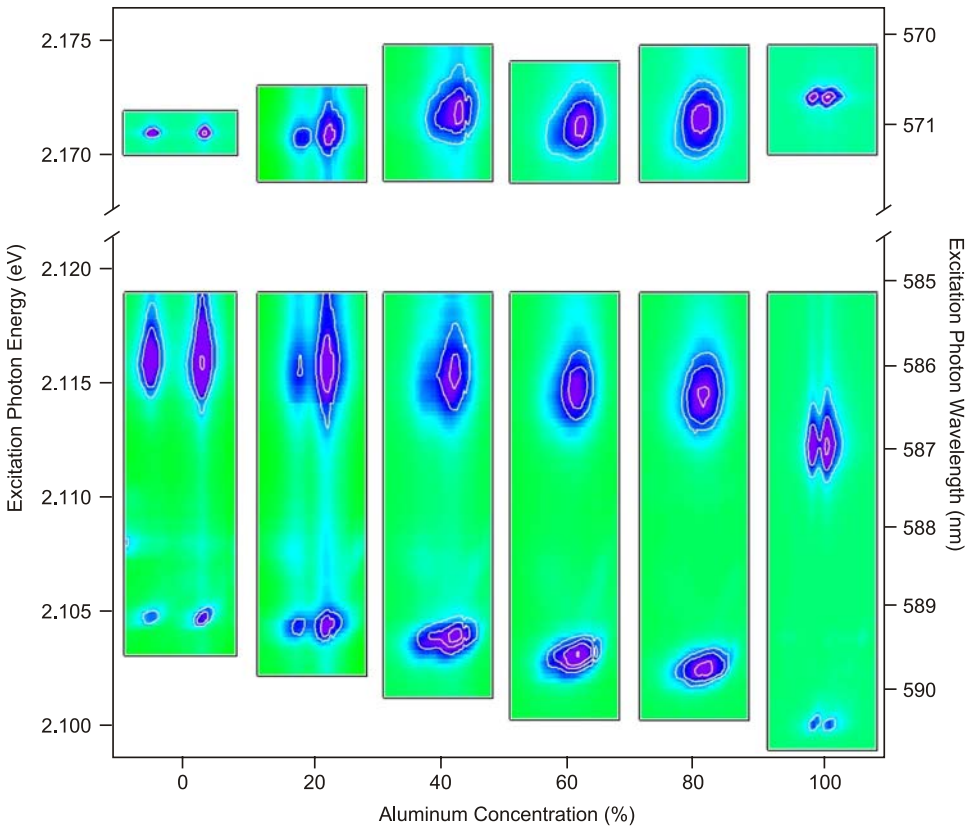

Fig. 8 Site-selective CEES images obtained from resonant excitation of the $^5D_0$ to $^7F_0$ europium transition and looking at the $^5D_0$ to $^7F_2$ emission of a series of europium-doped $Al_xGa_{1-x}N$ samples with varying aluminum content. The samples were grown by OMVPE and implanted with Eu^{2+} ions. The peaks occurring at the lowest excitation energy correspond to zero phonon emission, those occurring at the middle excitation energy correspond to the localized phonon sideband emission, and the peaks occurring at highest excitation energy correspond to the GaN LO phonon sideband emission

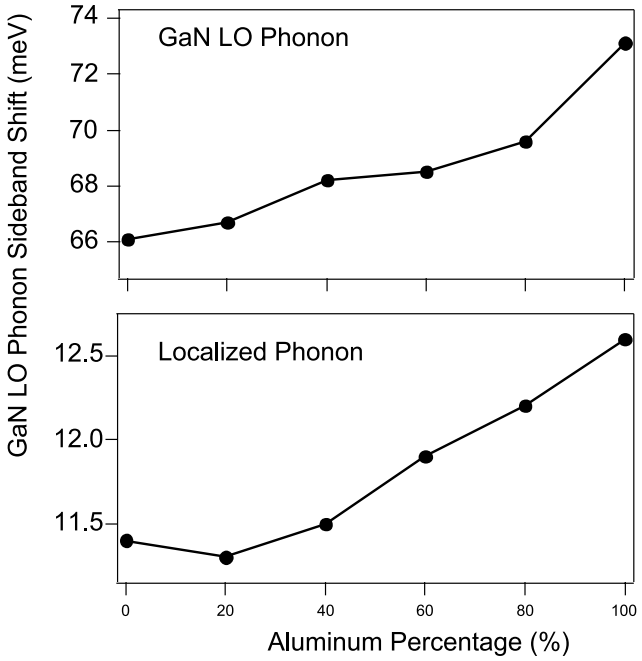

Fig. 9 LO phonon sideband and localized phonon sideband energy shifts as a function of aluminum concentration in $Al_xGa_{1-x}N$. The samples were grown by OMVPE and implanted with Eu^{2+} ions

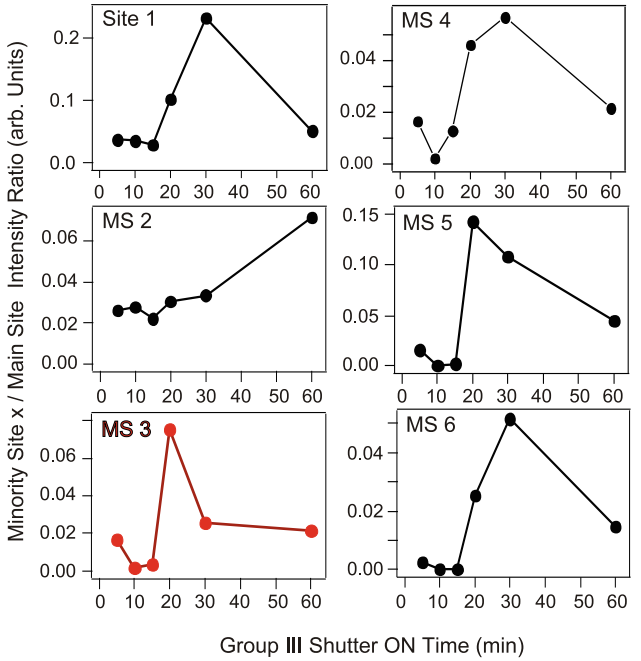

Fig. 10 Relative numbers of sites obtained for different Ga shutter-open times in the IGE growth method (Sample Type 1) for Eu-doped GaN

the perturbations, and hence the electron–phonon coupled transitions are relatively less pronounced. The energy shift relative to the zero-phonon lines increases for both modes as shown in Fig. 9. This is, for the LO mode, consistent with what is found in Raman spectroscopy as well. This gives us a solid confirmation of the assignment. It should be noted that Peng et al. [7] also observed shifts of about 12 meV, which they however assigned to additional sites. In view of our assignment, their result may have to be revisited and reinterpretation might be necessary to take the electron–phonon coupling into consideration.

Inspecting more closely the excitation spectrum for MS 6, we find that two peaks exist as well (see Table 1), which we can again explain by electron–phonon coupling. The local mode that is involved for this site has thus an energy of 8 meV.

3.3 Variation of growth conditions

With the fingerprints of our sites at hand, we can turn our attention to the variation in site incorporation as growth parameters are varied. In this section, we will look first at a series of samples (Sample Type 1) produced by IGE, which was designed to optimize the GaN growth conditions for efficient rare earth luminescence.

We find a strong variation of the relative abundance of the various sites. Since we expect that the total number of the main sites is not changing drastically, we take it as the reference and depict in Fig. 10 the relative PL intensities of the various sites as a function of time that the Ga beam is open during each cycle. The data show considerable scatter and no systematic behavior appears at first sight. It appears at least that MS 1, 3, 4, 5, 6 show a fairly similar dependence while MS 2 exhibits a different behavior. The first group has a maximum for a shutter-open time of about 20 min, while MS 2 increases continuously with shutter-open time.

Next, we turn our attention to the MBE-grown samples on sapphire (Sample Type 2). In Fig. 11, we depict the CEES data for the higher energy range of the $^5D_0$ to $^7F_2$ transition and compare it with the MBE-grown sample on silicon (Sample Type 1). We see immediately several clear differences. The trend that MS 2 is increased is even more pronounced than in the IGE series and exhibits about 20% of the emission intensity compared to the main site. Other sites are very weak and much less pronounced than in the IGE sample. In particular, MS 3 is hardly present. In addition to these differences in incorporation, the spectral widths of the transitions are significantly increased, making the peaks less distinct. Apparently, there are more perturbations and build-in strains in the samples grown on sapphire. This difference may be due to the substrate but also due to the difference in growth conditions and surface preparation. A similar behavior has been observed for Er-doped samples as well [12]. The exact same samples of Type 2 also have been studied for their magnetic properties. In these studies, an anti-correlation between remnant magnetization and PL intensity was found under variation of the Ga flux [17]. This poses questions as to whether the magnetization is related with a

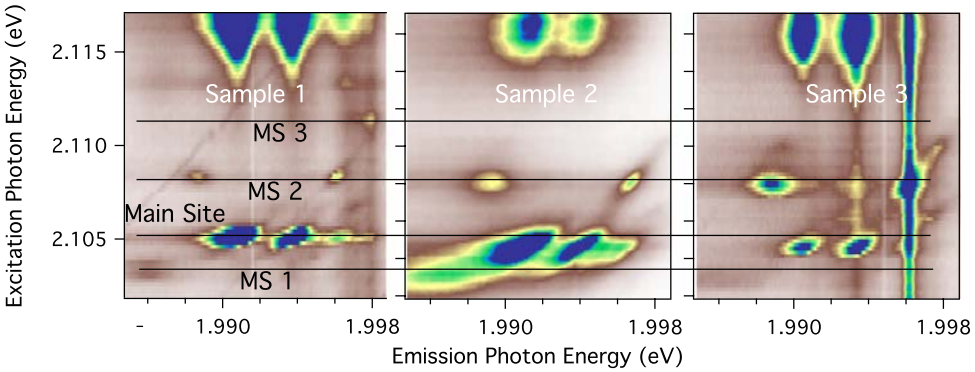

Fig. 11 Comparison of CEES data obtained for the three different types of Eu-doped GaN samples. Sample 1: regular MBE sample grown on glass. (Sample 1, 60 min.) Sample 2: regular MBE sample grown on sapphire. Sample 3: ion-implanted OMVPE grown sample

particular minority site. However, in our CEES studies none of the identified sites correlate positively with the magnetization.

In another variation of the growth and doping parameters, we investigated samples that have been grown by MOCVD on sapphire but doping was achieved by ion implantation (Sample Type 3). In Fig. 11, we compare the CEES data with the other types of samples. It is immediately apparent that the number of sites is reduced compared to Sample Type 1 but some more features are present compared to Sample Type 2. More specifically, we see three main features: (1) the main site with its phonon-assisted excitation band; (2) the minority site 2, which is however even stronger than in Sample Type 2, and may hence be connected with the defects that are induced by implantation; (3) a very pronounced vertical stripe similar to, but at a different position, than that seen in Sample Type 1. We will discuss these phenomena in the next section.

3.4 Excitation mechanism under non-resonant excitation

Having obtaining a detailed fingerprint of the different incorporation sites, we discuss in this section how these sites are excited off-resonance. For this we studied four different excitation types:

- Far below the bandgap of GaN in the visible spectral region.
- Below, but fairly close to, the bandgap.
- Above bandgap excitation.
- Excitation by energetic electrons in a SEM.

Through the site specificity of our studies, we can relate these excitation channels and determine site-specific relative excitation efficiencies.

Non-resonant excitation in the visible

Besides the abundance of different incorporation sites seen in Sect. 3.1 and the phonon-assisted excitation peaks identified in Sect. 3.2, there is a third type of emission feature: vertical stripes occurring at 1.956 eV, 1.9627 eV, 1.9980 eV, 2.0018 eV, and 2.0039 eV for Sample Type 1. Careful inspection of the 1.9980 eV stripe shows that there are in fact two different peaks that are energetically close together associated with this emission: one at 1.9976 eV and the other at 1.9986 eV. Referring back to Table 1, we see that three of the emission energy peaks corresponding to these excitation stripes match exactly with the peaks defining MS 3. This becomes even more apparent when we compare in Fig. 12 the emission spectra of MS 3 with the spectra that are obtained non-resonantly in the visible red region. Within uncertainty due to the spectral overlap of different sites, the two spectra match very well.

We further find that the emission energy of the other stripes match up with the emission energy peak associated with MS 4 and MS 5. Apparently, MS 3, 4, and 5 can be excited non-resonantly in the visible while the other sites cannot be excited or are excited with very low efficiency. We suspect that deep traps are excited with visible light, which then can transfer their energy to the Eu^{3+} ion. The efficiency of the process suggests that the ions and the traps form complexes or are at least in close proximity to one another. In fact, the presence of the trap in the near vicinity will change the resonant excitation and emission properties of the rare earth ion such that we could identify them as individual different sites.

Looking more closely at the CEES data for the ion-implanted sample shown in Fig. 11, we also see a very pronounced vertical stripe at a position that overlaps with the higher energy emission line of MS 2. There is also an apparent resonance at the excitation energy of MS 2 but only for the higher energy emission line. Decomposing the emission spectra on resonance and off-resonance reveals a new site (MS 8) with a high-energy emission peak that strongly overlaps but is not identical to MS 2. Both MS 2 and MS 8 are dominantly present in ion-implanted samples, while MS 3 is more abundant in IGE grown in situ doped samples on silicon (Sample Type 1). This has to be kept in mind when conclusions are drawn between in situ doped samples and ion-implanted samples. Differences of that kind have also

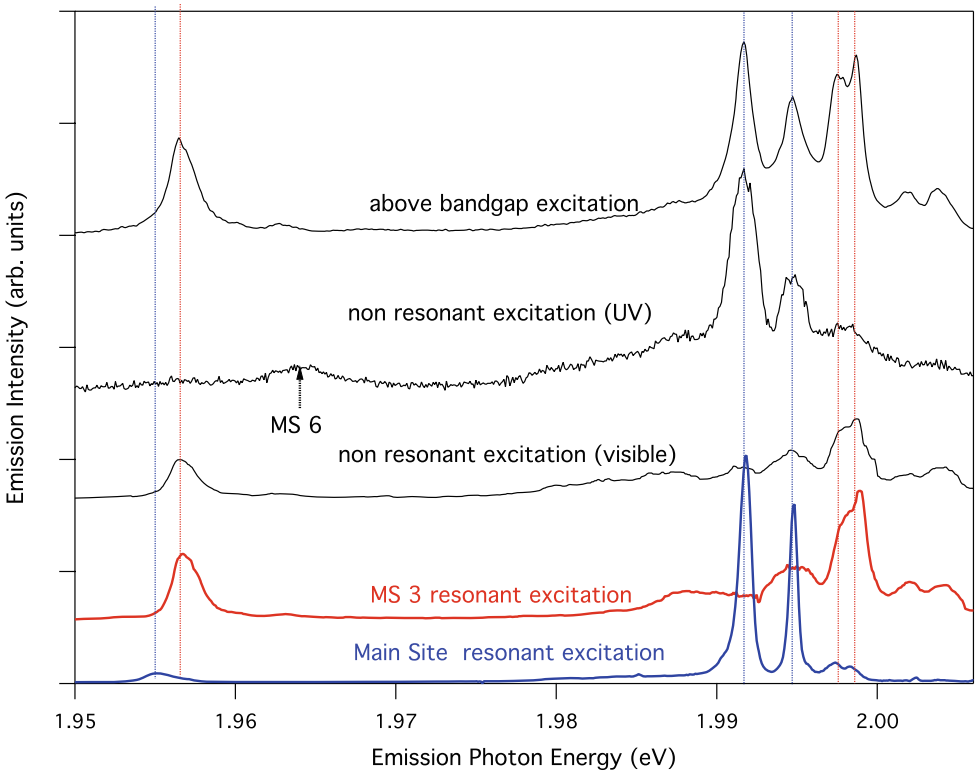

Fig. 12 Comparison of emission spectra obtained under different resonant and non-resonant excitation energies: MS 1 resonant excited at 2.1059 eV, MS 3 resonant at 2.1124 eV, non-resonant visible excitation at 2.1024 eV, non-resonant UV excitation at 3.06 eV and above bandgap excitation at 3.53 eV. Measurements were obtained for regular MBE sample grown on glass

been noticed in [10], where for both in situ doped and ion-implanted samples a site Eu_1 has been found which corresponds to our main site. In that work, they also found a second site in each type of sample (Eu_{2M}, Eu_{2I}), which however are different from each other. They can be correlated to our assignments as follows: Eu_{2M} = MS 3 and Eu_{2I} = MS 8.

Broad below-gap excitation bands in the visible were also observed for Er-doped GaN [21, 22] and were also attributed to excitation mediated through deep impurity- or defect-related traps. This shows that a visible non-resonant excitation channel is not unique to the Eu ion. The spectral position of the non-resonant excitation bands raises the suspicion that the defect traps may be related to the defects that cause the yellow emission in GaN (see e.g. [23–25]), which has been associated with intrinsic nitrogen vacancies [26, 27], or may be related to Eu ions in the vicinity of nitrogen vacancies. It is well known that shallow traps with emission features close to the band edge exist in GaN as well. Hence, we also explored the possibility of exciting the RE ions close to the bandgap.

Excitation close to the bandgap

Wang et al. performed PLE measurements in the band edge region on peaks associated with both the main site and the defect-related minority site MS 3 [28]. Their PLE spectra illustrated how the emission of our MS 3 site drops sharply for excitation energies just below the band edge at 3.4 eV. The main site continues to emit in the region between 3.0 eV and 3.4 eV. Similar results were reported by Peng et al. [7]. This observation provides clear evidence that different excitation pathways are at play for these two types of sites. In order to relate these observations more closely with our site-selective measurements, we measured an emission spectrum under below bandgap excitation using a GaN-based semiconductor laser emitting at 3.06 eV (405 nm). This spectrum is included in Fig. 12, allowing comparison of the emission produced by the two non-resonant excitation pathways. The differences are drastic, and it appears that sites that are excited through one channel are not excited through the other. We find that the main site and MS 1 are excited efficiently with the sub-bandgap UV light while MS 3, 4, and 5 are excited through visible light. Another feature at around 1.968 eV becomes apparent which matches MS 6 identified above. It is most apparent in IGE samples with Ga-shutter-open times larger than 20 min and can be observed in the MBE-grown sample. The enhancement of emission through near-band edge excitation for MS 6 is very strong such that we suspect that it is directly connected with a shallow trap just as MS 3 is related to a deep trap. Based on these results, the relative strength for different growth conditions, and the spectral positions allow us to correlate the sites from Peng's study [7] with ours. Their Site 1 corresponds to our main site, while their Site 2 corresponds to MS 3. Somewhat more tentatively, we assign their Site 3 to our MS 6. Their Site 4 may include some contributions from an electron–phonon

coupled transition of the main site and may hence not be an independent site.

Above bandgap excitation

Finally, we turn now to the excitation with light with photon energies above the bandgap of GaN, which is crucial to understand the issues that limit the performance of electroluminescence devices such as the excitation pathways from electron-hole pairs of the GaN host to the rare earth ion. The spectrum shown in Fig. 12 was obtained under above bandgap excitation (3.53 eV, 351 nm) for our MBE sample. By comparison with the emission spectra under direct resonant excitation, we find that, in addition to the main site, minority sites MS 3, 4, and 5 which are related to deep defect traps dominate the emission spectra. Closer inspection also reveals contributions from the other minority sites that are related to shallow traps. In any case, the main site is much less dominant in the above bandgap excitation, suggesting that the excitation efficiency of the minority sites is enhanced compared to the main site. We quantify this statement in Table 2, in which we list the relative emission strength of each minority site in comparison to the main site for both the resonant and the above bandgap excitation scheme.

The MS 3 has a significantly higher excitation efficiency compared to the main site quantified by the enhancement factor in Table 2. This factor becomes even higher (up to 60) for some of the other samples that we studied. Because it is just a relative measure, it is unclear if this sample dependence is due to a change in efficiency of MS 3 or of the main site.

We also note that we cannot find any spectral feature associated with site MS 2 and hence conclude that this incorporation site can only be excited resonantly. It appeared quite strongly in our ion-implanted sample, but even there it was absent from the above bandgap excitation spectra. This gives first evidence that not every ion can be excited through the creation of electron-hole pairs. In particular, MS 2 has to be avoided in the ion-implanted samples. Similar conclusion have been drawn by O'Donnell and his group [29].

Table 2 Relative percentage of the indicated minority site emission with respect to majority site emission for resonant excitation and above bandgap excitation. Error estimates for these values are ±0.5 percent. An enhancement factor is calculated as the ratio of the two numbers above. Data were obtained for the MBE-grown sample

	MS 1	MS 3	MS 4	MS 5	MS 6	MS 7
Above bandgap	18.2	103.7	11.1	6.4	1.8	1.6
Resonant excitation	9.3	5.3	2.6	4.0	1.4	1.3
Enhancement factor	2	19.5	4.2	1.6	1.3	1.2

Excitation through energetic electrons

As a final method of exciting the rare earth ions, we have used the electron beam in a SEM instrument and measured the resulting cathodoluminescence. For weak excitation density the emission spectra resemble those from above band gap excitation, suggesting that excitation through the creation of electron-hole pairs by the impinging electrons is the main excitation pathway. In the SEM, we have the opportunity to increase the excitation density such that saturation can be achieved. Under such conditions, we would expect that all possible ions are excited and hence the emission is coming dominantly from the main site. However, we find that the emission intensity from site MS 3 and the main site are still almost equal [9]. From this we have to conclude that not all ions that we see as the main site in resonant excitation can be excited in this way. A similar conclusion was obtained from saturated PL measurements in [10].

Excitation model for non-resonant excitation

Based on the data observed so far, it is apparent that there are two dominant excitation pathways that account for the majority of the above bandgap Eu emissions. Both of these pathways involve Eu excitation by a trap-mediated energy transfer process. Shown in Fig. 13 is a schematic representation of these two dominant excitation pathways labeled Shallow Trap Excitation Pathway (corresponding to the MS 1 and main site excitation) and the Deep Trap Excitation Pathway (corresponding to excitation of MS 3, 4, and 5). In both pathways, we assume that under above bandgap excitation an electron-hole pair is created first which then transfers the energy to the respective defect trap. From there, energy can be transferred to the rare earth ion through most likely an Auger process [30, 31]. There may be several kinds of each type of defect trap, and some of them may be directly related intrinsically with the Eu ions. In particular, we assume this to be the case for MS 3 and MS 6 for which a very efficient excitation is possible after excitation of the traps. However, the two are clearly distinct. On the other hand, it is also possible that some Eu incorporation sites that do not act as traps themselves can be excited through a defect trap in their vicinity. The distance from such defect traps will then govern the excitation efficiency and some ions may be too far away to be excited at all. This interpretation explains that not all main sites and essentially none of MS 2 can be excited through electron-hole pairs.

4 Summary and conclusion

We have identified through resonant excitation at least nine different incorporation sites of Eu ions in GaN and studied how these sites behave under different excitation conditions and how their relative number is modified by different

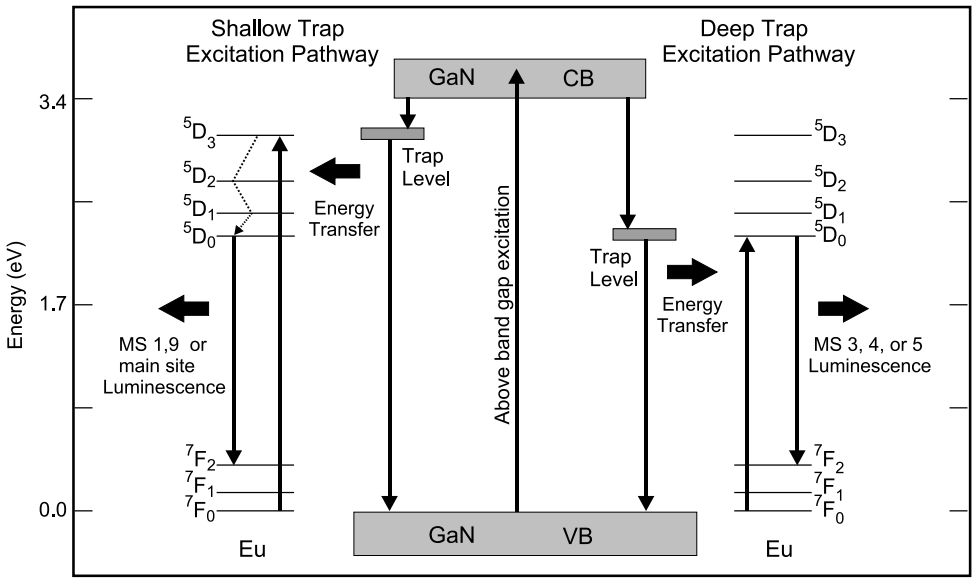

Fig. 13 Simple excitation model for rare earth ions after excitation of electron-hole pairs

growth and doping conditions. For the latter, we find that a main site (most like a fairly unperturbed Eu ion on Ga site) is always dominant while the minority sites change substantially in relative numbers and can come close (MS 2) in ion-implanted samples. In terms of the excitation pathway after the creation of electron-hole pairs, we found three types of centers: (1) MS 1, MS 6, and the main site which are excited through shallow traps; (2) MS 3, 4, 5, and 8 which are excited through the deep traps; (3) some sites like MS 2 and a large fraction of the main site that cannot be excited at all. We interpret this finding by the fact that the ion by itself is not very efficient in trapping excitation and that its excitation involving other traps depends on the ion/trap distance. Many of the main sites are far away from these traps and cannot be excited through this channel at all. The relative number for the remaining sites is too small to decide on their excitation pathway.

The most efficient excitation channel involves deep-trap states. Unfortunately, the corresponding rare earth ion sites are not very abundant. The deep-trap states are not uniquely defined, since at least for Eu several sites are observed that are excited this way. In particular, in ion-implanted and in situ doped samples the dominant defect related sites are quite distinct from each other (MS 3 vs. MS 8). The presence of rare earth ions that cannot be excited efficiently through electron-hole pairs poses a significant hurdle for the realization of electrically pumped RE-based GaN lasers due to the added loss that they will represent. In enriching the defect-related incorporation sites for improved performance of light emitting devices, one is faced however with the limitation of growth parameters and the requirement that the active layers must still be viable to be used in an injection-type or p–n junction-type device. As shown in this paper, the IGE process is a method for achieving this compromise. The improvement in luminescence obtained in IGE-grown samples is thought to be related to the nitridation process which takes place during the OFF (i.e. N-only) cycle. Munasinghe and Steckl [3] have shown that conventionally MBE-grown samples display an increase in PL intensity when exposed to N at high temperature after growth. By comparison, there was no change in PL for samples that were maintained at high temperature after growth but without N flow (essentially in situ annealing). Therefore, the amount of N incorporated into the GaN films is clearly a critical parameter in both defect concentration and the PL efficiency. Unfortunately, optical studies are not used to determine which element causes a perturbation of the Eu^{2+} ion and hence do not allow for identification of the respective defect complexes. The IGE technique has the unique degree of freedom of being able to introduce additional N in the films during the non-growth OFF cycle while allowing the III/N ratio during the ON cycle to be set for enhancing the incorporation of Eu.

Acknowledgements The Lehigh part of this work has been supported by an NSF grant (DMR NSF-DMR-0705217), and collaborative agreement W911NF-07-2-0064 between the Army Research Lab and Lehigh University. The Cincinnati work was supported by a grant from the U.S. Army Research Office (W911NF-06-1-0296).

References

1. A.J. Steckl, J.C. Heikenfeld, D.S. Lee, M.J. Garter, C.C. Baker, Y.Q. Wang, R. Jones, Rare-earth-doped GaN: Growth, properties, and fabrication of electroluminescent devices. IEEE J. Sel. Top. Quantum Electron. **8**, 749–766 (2002)
2. J.H. Park, A.J. Steckl, Laser action in Eu-doped GaN thin-film cavity at room temperature. Appl. Phys. Lett. **85**, 4588–4590 (2004)
3. C. Munasinghe, A.J. Steckl, GaN: Eu electroluminescent devices grown by interrupted growth epitaxy. Thin Solid Films **496**, 636–642 (2006)

4. J.H. Park, A.J. Steckl, Visible lasing from GaN: Eu optical cavities on sapphire substrates. Opt. Mater. **28**, 859–863 (2006)
5. J.H. Park, A.J. Steckl, Site specific Eu^{3+} stimulated emission in GaN host. Appl. Phys. Lett. **88**, 011111 (2006)
6. U. Hömmerich, E.E. Nyein, D.S. Lee, J. Heikenfeld, A.J. Steckl, J.M. Zavada, Photoluminescence studies of rare earth (Er, Eu, Tm) in situ doped GaN. Mat. Sci. Eng. B **105**, 91–96 (2003)
7. H. Peng, C. Lee, H.O. Everitt, C. Munasinghe, D.S. Lee, A.J. Steckl, Spectroscopic and energy transfer studies of Eu^{3+} centers in GaN. J. Appl. Phys. **102**, 073520 (2007)
8. L. Bodiou, A. Braud, J.L. Doualan, R. Moncorge, K. Lorenz, E. Alves, Two colour experiments in Eu^{3+} implanted GaN. J. Alloys Comput. **451**, 140–142 (2008)
9. S. Tafon Penn, Z. Fleischman, V. Dierolf, Site-specific excitation of Eu ions in GaN. Phys. Stat. Sol. (a) **205**(1), 30–33 (2008)
10. L. Bodiou, A. Braud, J.-L. Doualan, R. Moncorgé, J.H. Park, C. Munasinghe, A.J. Steckl, K. Lorenz, E. Alves, B. Daudin, Optically active centers in Eu implanted, Eu in situ doped GaN, and Eu doped GaN quantum dots. J. Appl. Phys. **105**, 043104 (2009)
11. G. Metcalfe, E. Readinger, P. Shen, N. Woodward, V. Dierolf, M. Wraback, Crystal-field split levels of Nd^{3+} ions in GaN measured by luminescence spectroscopy. J. Appl. Phys. **105**, 053101 (2009)
12. V. Dierolf, C. Sandmann, J. Zavada, P. Chow, B. Hertog, Site-selective spectroscopy of Er in GaN. J. Appl. Phys. **95**, 5464–5470 (2004)
13. H.J. Bang, S. Morishima, J. Sawahata, J. Seo, M. Takiguchi, M. Tsunemi, K. Akimoto, M. Nomura, Concentration quenching of Eu-related luminescence in Eu-doped GaN. Appl. Phys. Lett. **85**, 227–229 (2004)
14. E.E. Nyein, U. Hommerich, J. Heikenfeld, D.S. Lee, A.J. Steckl, J.M. Zavada, Spectral and time-resolved photoluminescence studies of Eu-doped GaN. Appl. Phys. Lett. **82**, 1655–1657 (2003)
15. H.Y. Peng, C.W. Lee, H.O. Everitt, D.S. Lee, A.J. Steckl, J.M. Zavada, Effect of optical excitation energy on the red luminescence of Eu^{3+} in GaN. Appl. Phys. Lett. **86**, 051110 (2005)
16. V. Dierolf, Z. Fleischman, C. Sandmann, A. Wakahara, T. Fujiwara, C. Munasinghe, A. Steckl, Combined excitation emission spectroscopy of europium ions in GaN and AlGaN films, in *Mater. Res. Soc. Symp. Proc.*, vol. 866, V3.6.1 (2005)
17. J. Hite, G.T. Thaler, R. Khanna, C.R. Abernathy, S.J. Pearton, J.H. Park, A.J. Steckl, J.M. Zavada, Optical and magnetic properties of Eu-doped GaN. Appl. Phys. Lett. **89**, 132119 (2006)
18. T. Fujiwara, A. Wakahara, Y. Nakanishi, A. Yoshida, Photoluminescence properties of Eu-implanted AlN. Phys. Stat. Sol. (c) 2805–2808 (2005)
19. T. Monteiro, C. Boemare, M.J. Soares, R.A.S. Ferreira, L.D. Carlos, K. Lorenz, R. Vianden, E. Alves, Photoluminescence and lattice location of Eu and Pr implanted GaN samples. Physica B **308**, 22–25 (2001)
20. M. Pan, A.J. Steckl, Red emission from Eu-doped GaN luminescent films grown by metalorganic chemical vapor deposition. Appl. Phys. Lett. **83**, 9–11 (2003)
21. S. Kim, S.J. Rhee, D.A. Turnbull, E.E. Reuter, X. Li, J.J. Coleman, S.G. Bishop, Observation of multiple Er^{3+} sites in Er-implanted GaN by site-selective photoluminescence excitation spectroscopy. Appl. Phys. Lett. **71**, 231–233 (1997)
22. S. Kim, S.J. Rhee, X. Li, J.J. Coleman, S.G. Bishop, P.B. Klein, Excitation mechanisms of multiple Er^{3+} sites in Er-implanted GaN. J. Electron. Mater. **27**, 246–254 (1998)
23. R. Singh, R.J. Molnar, M.S. Unlu, T.D. Moustakas, Intensity dependence of photoluminescence in GaN thin films. Appl. Phys. Lett. **64**, 336–338 (1994)
24. C.H. Chiu, F. Omnes, C. Gaquiere, P. Gibart, J.G. Swanson, The GaN yellow luminescence centre observed using optoelectronic modulation spectroscopy. J. Phys. D, Appl. Phys. **35**, 609–614 (2002)
25. M.H. Zaldivar, P. Fernandez, J. Piqueras, Influence of deformation on the luminescence of GaN epitaxial films. Semicond. Sci. Technol. **13**, 900–905 (1998)
26. H.M. Chen, Y.F. Chen, M.C. Lee, M.S. Feng, Yellow luminescence in n-type GaN epitaxial films. Phys. Rev. B **56**, 6942–6946 (1997)
27. J. Bernholc, J.C. Chervin, A. Polian, T.D. Moustakas, Towards the identification of the dominant donor in GaN. Phys. Rev. Lett. **75**, 296–299 (1995)
28. K. Wang, R.W. Martin, K.P. O'Donnell, V. Katchkanov, Selectively excited photoluminescence from Eu-implanted GaN. Appl. Phys. Lett. **87**, 1121072 (2005)
29. K.P. O'Donnell, Private communication at MRS (2008)
30. W. Fuhs, I. Ulber, G. Weiser, M.S. Bresler, O.B. Gusev, Excitation and temperature quenching of Er-induced luminescence in a-Si: H (Er). Phys. Rev. B **56**, 9545–9551 (1997)
31. N. Yassievich, M.S. Bresler, O.B. Gusev, Defect-related Auger excitation of erbium ions in amorphous silicon. J. Phys. Condens. Matter. **9**, 9415 (1997)